Identification of Reaction Mechanisms with a Dynamic PFR Model ⋆

Jan C. Schöneberger * **Harvey Arellano-Garcia** *
Holger Thielert ** **Günter Wozny** *

* *Berlin Institute of Technology,Chair of Process Dynamics and Operation, Berlin, Germany (e-mail: jan.schoeneberger@tu-berlin.de)*
** *Uhde GmbH, Dortmund, Germany*

Abstract: In this work, a dynamic model of a catalytic fixed bed reactor (FBR) based on partial differential equations (PDE) is introduced and used for the identification of reaction mechanisms which take place during the oxidation of sulfur dioxide over a vanadium pentoxid catalyst. The measured data is collected from a pilot plant, which uses commercial sized catalyst particles. In order to reduce the experimental effort, a developed framework based on the methods of nonlinear optimal experimental design is applied using a steady state FBR model. The systematic procedure is improved using a dynamic reactor model. This makes the time dependent measurement data valuable for the identification procedure.

Keywords: Catalytic fixed bed reactor (FBR), reaction mechanisms, partial differential equations (PDE), parameter identification, optimal experimental design.

1. INTRODUCTION

Catalytic gas phase reactions have a high relevance in chemical engineering. The majority of chemical processes will not be profitable and in some cases not even viable without the usage of catalysts. An important application represents the utilization of FBR for waste gas treatment processes. In this work, the oxidation of sulfur dioxide to sulfur trioxide is considered, which is converted with water to sulphuric acid. It should be noted that huge effort is made in the development of new catalysts with a higher activity. Commonly, new catalysts are designed and tested at micro scale, i.e. a pulverized catalyst. However, the catalyst used in industrial plants are much larger and the previously identified mechanisms and kinetic parameters can not be transferred without further investigations in a scale up procedure w.r.t. the reactor layout. Thus, measurements with commercial catalyst particles are inevitable implying a high experimental effort. The sized particles require a larger reactor diameter, and thus, high gas flow rates are necessary in order to hold the operation conditions close to the industrial scale reactor. Moreover, corresponding requirements for process automation and safety engineering have to be met. Consequently, in order to reduce the experimental effort while reaching a desired model quality, methods of nonlinear optimal experimental design can be applied. In addition, due to the fact that a good deal of data enhances the mechanism and parameter identification, the proposed framework can still be improved when using a model, which describes the pilot plant dynamic behavior. In this work, a homogeneous and a two-phase FBR model are presented. The latter can be used for dynamic simulations. Both are compared to each other based on a set of measured data taken from an identification campaign. The experiments were performed in a pilot plant (Fig. 1) using a commercially available vanadium pentoxid catalyst.

⋆ This work is supported by the Max-Buchner-Forschungsstiftung.

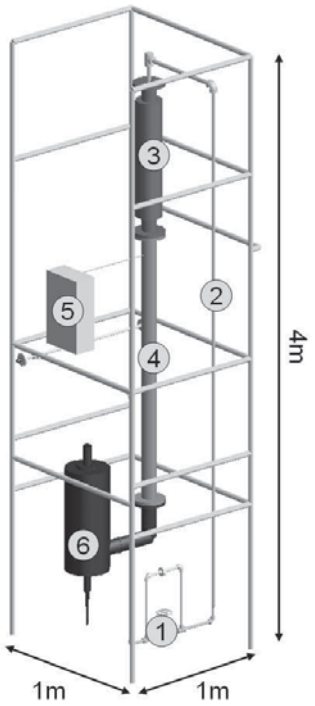

Fig. 1. Pilot plant set-up: (1) Quality measurement, (2) Heating section, (3) Reactor, (4) Tube bundle cooler, (5) Quality measurement, (6) Bubble column.

2. PILOT PLANT DESCRIPTION

The core of the pilot plant is the tubular reactor which has a diameter of $D_R = 0.1$ m and a length of $L_R = 1$ m.

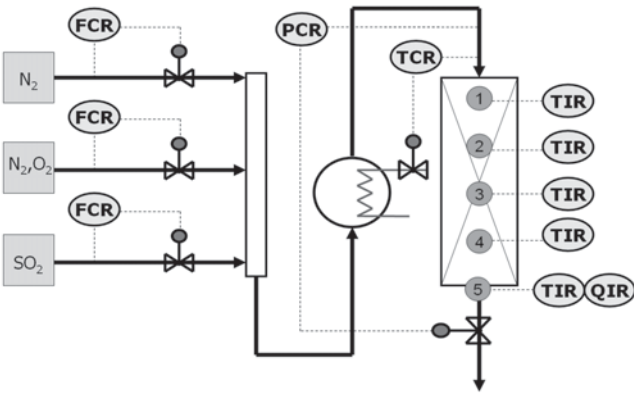

Fig. 2. Control structure: (FCR) Flow control and measurement, (TCR) Temperature control and measurement, (PCR) Pressure control and measurement, (TIR) Temperature measurement, (QIR) Quality measurement.

The diameter results from the size of the catalyst particle, which is about $D_P = 0.005$ m for the examined catalyst. It represents the minimum diameter required in order to get a uniform particle distribution. The reactor consists of five beds of catalyst packing, where each is $H_B = 0.1$ m high. The additional length is used to reduce in and outlet effects. The reactor is operated nearly adiabatic using an electric heated isolation. The majority of the available space is occupied by the secondary units such as the heating, cooling and gas scrubbing. The last two steps are combined in a bubble column. Fig. 1 gives an idea of the pilot plant set-up. The pilot plant is automated using ABB Freelance. Beside the implemented safety engineering procedures, the reactor inlet variables are controlled using the structure given in Fig. 2. The gas flow rate $\dot{V}$ can be varied between 200 and 400 norm liter per minute at inlet temperatures up to $T_{in} = 500$°C.

3. REACTOR MODELS

Two reactor models are presented, which describe the FBR behavior, namely the *homogeneous model* and the *two-phase model*. The chemical reaction is modeled with six different reaction mechanisms for which several steps of parameter identification and model discrimination are performed in order to find the best suitable mechanism. Besides the kinetic parameters in the reaction rate equations, the reactor models contain several parameters. Some of them can be obtained from the particles geometry e.g. the packing porosity ϵ, the relative particle diameter D_P, the specific surface area a, and the catalyst density ρ_C, other parameters are derived from property functions such as the component heat capacities $c_{P,i}$ and $c_{V,i}$, the heat of reaction Δh_R, and the thermodynamic equilibrium constant, K_P. The heat loss can be determined from experimental runs without reactions and is then calculated with the estimated heat transfer coefficient, k_W, and the measured wall temperature, T_W. Four components are considered in the model with the indices as given in Tab. 1.

Table 1. Component indices

Index	1	2	3	4
Component	**SO_2**	**O_2**	**SO_3**	**N_2**

3.1 Homogeneous Model

The model equations composed of mass balances, (1), energy balance, (2), and momentum balance, (3), imply the assumption of a plug flow profile in the reactor and an instant heat and mass transfer between the gas and the solid phase. This means that the temperature of the catalyst particle is the same as the gas phase bulk temperature. Due to this issue the model can not be used for the description of the dynamic behavior, since the heat capacities of gas and solid differ a lot. A detailed description and derivation of the homogeneous model can be found in Arellano-Garcia et al. (2007).

$$\frac{dF_i}{dz} = \nu_i \dot{r} \cdot \rho_C (1-\epsilon) \frac{\pi}{4} D_R^2 \tag{1}$$

$$\frac{dT}{dz} = \frac{-\dot{r}\Delta h_R(T)\rho_C(1-\epsilon)\frac{\pi}{4}D_R^2 - k_W \pi \; D_R \, (T - T_W)}{\sum F_i c_{P,i}} \tag{2}$$

$$\frac{dP}{dz} = -\frac{\sum F_i M_i}{\rho \frac{\pi}{4} D_R^2 D_P} \left(\frac{1-\epsilon}{\epsilon^3}\right) \cdot \left[\frac{150(1-\epsilon)\eta}{D_P} + 1.75 \frac{\sum F_i M_i}{\frac{\pi}{4} D_R^2}\right] \tag{3}$$

In the model equations, F_i denotes the component flow rates, ν_i the stoichiometric coefficient, and M_i, the molar mass. T stands for the gas and the catalyst temperature, P for the gas phase pressure. The viscosity η is calculated assuming an ideal mixing.

Following the simulation results based on this model, the pressure drop can be neglected for the given reactor set-up and is not considered anymore in the two-phase model.

3.2 Two-Phase Model

The key idea of developing a two-phase model is to perform dynamic simulations of the reactor behavior in order to include time variant measurement data in the parameter estimation procedure. Due to the varieties in the resulting time constants in the energy balances, which are mainly influenced by the heat capacity and density in its corresponding phase, a split modeling of the gas and solid phase becomes inevitable. The resulting equation system comprises mass and energy balances for the two phases,(4)- (7), which are coupled via mass and heat transfer correlations,(8)-(10). Instead of the component flow rates (see (1)), the concentrations in the gas phase $c_{G,i}$ and the solid phase $c_{C,i}$ are used here as state variables.

$$\frac{dc_{G,i}}{dt} = D_{ax_i} \frac{\partial^2 c_{G,i}}{\partial z^2} - \frac{\dot{V}}{\epsilon \frac{\pi}{4} D_R^2} \frac{\partial c_{G,i}}{\partial z} - a \frac{1-\epsilon}{\epsilon} \beta (c_{G,i} - c_{C,i}) \tag{4}$$

$$\frac{dc_{C,i}}{dt} = \nu_i \dot{r} \rho_k + a \, \beta (c_{G,i} - c_{C,i}) \tag{5}$$

$$\sum_{i=1}^{4} c_{G,i} c_{V_i} \frac{dT_G}{dt} = a \frac{1-\epsilon}{\epsilon} \alpha (T_C - T_G) - \frac{\dot{V}}{\epsilon \frac{\pi}{4} D_R^2} \cdot \sum_{i=1}^{4} c_{G,i} c_{P_i} \frac{\partial T_G}{\partial z} - k_W \frac{4}{\epsilon \; D_R} (T_G - T_W) \tag{6}$$

$$\frac{dT_C}{dt} = \frac{a\alpha}{\rho_C c_{P,C}} (T_G - T_C) - \frac{\Delta h_R \dot{r}}{c_{P,C}} \tag{7}$$

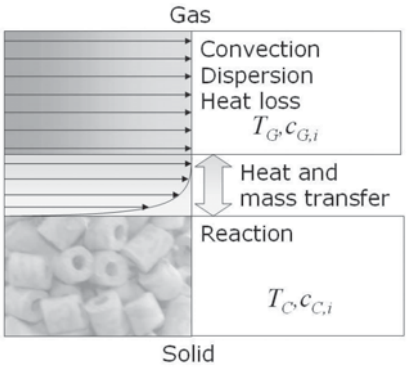

Fig. 3. Control volume of the two-phase model.

The control volume and the considered state variables of the two phases are shown in Fig. 3. The transfer coefficients (α, β, D_{ax}) are calculated with dimensionless numbers (Nusselt number Nu, Sherwood number Sh, axial Peclet number Pe_{ax}) and correlations taken from literature, see e.g. Fogler (2006). Here, $D_{ab,i}$ stands for the diffusion coefficient of the component i in nitrogen and $\bar{\lambda}$ for the mixtures heat conductivity.

$$D_{ax} = \frac{\dot{V} D_P}{Pe_{ax} \epsilon \frac{\pi}{4} D_R^2} \tag{8}$$

$$\beta_i = \frac{Sh_{\epsilon,i}\, D_{ab_i}}{D_P} \tag{9}$$

$$\alpha = \frac{\bar{\lambda} Nu}{D_P} \tag{10}$$

On the one hand, a dynamic simulation becomes possible with the inclusion of the solid phase, but on the other hand, new unknown or not well-known parameters are introduced. Three parameters are used in the transport correlations, one for each equation. In addition, two parameters depend on the catalyst particle properties, namely, the catalyst heat capacity, $c_{P,C}$, and the specific surface area, a. These additional parameters are to be determined from the measurement data, but they are strong correlated with the reaction rate, and thus, with the kinetic parameters of the reaction mechanisms. This problem can be overcome by running experiments without a reaction, i.e. with pure nitrogen or air. By this means the parameter in the heat transfer correlation, and the catalyst properties can be determined independently.

3.3 Reaction Mechanisms

In the open literature, plenty of different reaction mechanisms have been published for the oxidation of sulfur dioxide over vanadium pentoxid, we refer to Mezaki and Kadlec (1972) for an overview. In this work, the five of the most promising rate laws are selected. Additionally, a generic power law mechanism is also considered. All the rate equations describe the reaction stated in equation (11). They are functions of the components partial pressures, P_i, and the temperature, T, which affects the calculation of the velocity constant k, and the equilibrium constants K_P, and K.

$$\mathbf{SO_2} \; + \; \frac{\mathbf{1}}{\mathbf{2}} \, \mathbf{O_2} \; \rightleftharpoons \; \mathbf{SO_3} \tag{11}$$

Power Law: In the rate equation for the power law mechanism (12), the component exponents a, b, and c are treated as model parameters and have to be determined from the measurements. The temperature dependent velocity constant k is calculated with equation (13), in which the kinetic parameters p_1 and p_2 have to be identified.

Rate 1:

$$\dot{r} = k \left(P_{SO_2}^a P_{O_2}^b P_{SO_3}^c - \frac{P_{SO_2}^{(a-2)} P_{O_2}^{(b-1)} P_{SO_3}^{(c+2)}}{K_P} \right) \tag{12}$$

$$k = exp\left(\frac{p_1}{T} + 0.5 \; ln(T) + p_2 \right) \tag{13}$$

Mechanistic Rate Equations: The rate equations (14) to (18) can be derived assuming a liquid metal phase on the catalyst particle formed by vanadium, in which the supplied oxygen is dissolved. This is a widely accepted assumption for the oxidation over vanadium pentoxid. The differences in the reaction rates result from different mechanisms of the catalyst activation with oxygen.

Rate 2:

$$\dot{r} = \frac{k K P_{SO_2} P_{O_2}^{1/2}}{\left[P_{SO_3}^{1/2} + (K P_{SO_2})^{1/2} \right]^2} \left(1 - \frac{P_{SO_3}}{K_P P_{SO_2} P_{O_2}^{1/2}} \right) \tag{14}$$

Rate 3:

$$\dot{r} = \frac{k K P_{SO_2} P_{O_2}}{\left[P_{SO_3}^{1/2} + (K P_{SO_2})^{1/2} \right]^2} \left(1 - \frac{P_{SO_3}^2}{K_P^2 P_{SO_2}^2 P_{O_2}} \right) \tag{15}$$

Rate 4:

$$\dot{r} = \frac{k K P_{SO_2} P_{O_2}^{1/2}}{\left[P_{SO_3}^{1/2} + (K P_{SO_2})^{1/2} \right] P_{SO_3}^{1/2}} \left(1 - \frac{P_{SO_3}}{K_P P_{SO_2} P_{O_2}^{1/2}} \right) \tag{16}$$

Rate 5:

$$\dot{r} = \frac{k \left(K P_{SO_2} \right)^{1/2} P_{O_2}}{\left[P_{SO_3}^{1/2} + (K P_{SO_2})^{1/2} \right]} \left(1 - \frac{P_{SO_3}^2}{K_P^2 P_{SO_2}^2 P_{O_2}} \right) \tag{17}$$

Rate 6:

$$\dot{r} = \frac{k K P_{SO_2} P_{O_2}}{\left[P_{SO_3}^{1/2} + (K P_{SO_2})^{1/2} \right] P_{SO_3}^{1/2}} \left(1 - \frac{P_{SO_3}^2}{K_P^2 P_{SO_2}^2 P_{O_2}} \right) \tag{18}$$

All these rate equations utilize the same approach for the velocity constant k, and the equilibrium of the vacant sites K, which are given in the equations (19) and (20).

$$k = exp\left(p_1 - \frac{p_2}{T} \right) \tag{19}$$

$$K = exp\left(p_3 - \frac{p_4}{T} \right) \tag{20}$$

3.4 Numerical Solution

In order to keep the computational effort low, both reactor models were discretized using the orthogonal collocation (OC), see Schöneberger et al. (2009). In the case of the homogeneous model this leads to an algebraic equation system (AE) and in the case of the two-phase model to a system of ordinary differential equations (ODE). The

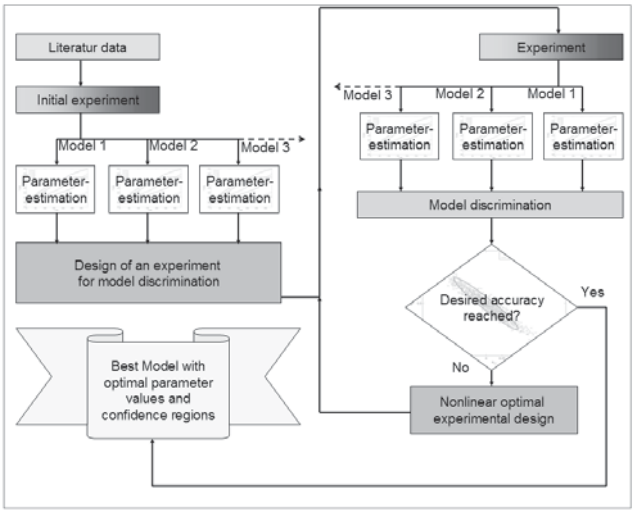

Fig. 4. Model identification framework.

AE is solved with a Newton-Raphson step and the ODE is integrated with an OC based Runge-Kutta algorithm. The use of the numerical solution in an optimization framework requires a very robust solution algorithm, in particular, when the free variables are positioned in exponential terms such as in the case of kinetic parameter estimation. Therefore, specialized initial value generation algorithms and step size control algorithms are required, see Schöneberger et al. (2007). Anyhow, the solution of the homogeneous model is more robust. Consequently, the first parameter estimation is performed with this model in order to get good initial parameter values for the two-phase model.

4. MECHANISM IDENTIFICATION FRAMEWORK

The proposed framework in Fig. 4 is based on the methods of nonlinear experimental design. It is similar to the model building framework proposed by Franceschini and Macchietto (2008), but with some improvements regarding the specific problem. There is only one experiment designed for model discrimination, and this is performed in the beginning of the identification procedure. Further experiments are exclusively designed in order to improve the parameter accuracy until the parameter spreading is in an acceptable region. Please note that all six reaction rates are considered in the steps 'Parameter estimation' and 'Model discrimination' of the loop in Fig. 4, but the 'Nonlinear optimal experimental design' is only performed for the actually best rate model.

4.1 Parameter Estimation Problem

The objective of the parameter estimation procedure is to find the parameter values which set the numerical solution of the model equations (e.g. (1), (2), and (3) for the homogeneous model) as close as possible to the measured data. For this purpose, the problem (21), here stated for the homogeneous model, has to be solved. In this work, a weighted least square functional is used as objective function and it's final value is named LSQ. High values are related to a high lack of fit.

$$\min_{p_1,p_2,a,b,c} \mathsf{LSQ} = \sum_{j=1}^{NM} \frac{\left(T_{ns,j} - T_{md,j}\right)^2}{\sigma^2_{T_j,T_j}} \tag{21}$$

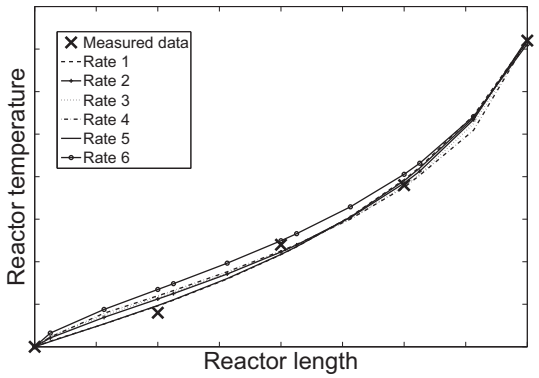

Fig. 5. Initial experiment.

In equation (21) the subscripts ns and md denote numerical solution and measured data, respectively, NM is the number of measured data points, and $\sigma^2_{T_j,T_j}$ is the standard deviation of the measured quantity (here the temperature T) at the measured point j. The calculated temperature profiles for the different rate laws after the parameter estimation are compared to the measured temperature data in Fig. 5. In Tab. 2, the LSQ values for the different rate models are given. All models are able to describe the measured data. This is not surprising, because 4 parameters (5 for rate 1) are fitted to only 5 measured points. Anyhow, the structure of the rate equations does not allow the same good fit for all rates. The best fit is reached with rate 5.
The parameter estimation problem becomes more difficult when more data points are available. The model equations have to be solved separately for each new experiment, making the parameter estimation the most expensive step regarding the computational effort.

Table 2. LSQ values for different rate models.

Rate	1	2	3	4	5	6
LSQ	0.488	0.688	0.821	0.916	0.461	1.901

4.2 Model Discrimination Problem

It is difficult to choose the best suitable rate model from Fig. 5. The discrimination step normally is performed taking the model with the lowest LSQ value. But, after only one experiment the models LSQ values are still close together, see Tab. 2. Thus, in a second step an experiment is designed that drift apart from the calculated temperature profiles for the estimated set of parameters. To do this, the optimization problem given in equation (22) is solved. By this means, the obtained inlet conditions are optimal for the discrimination step. Due to the fact that only one measured variable is considered, here a simpler formulation is chosen as proposed by Akaike (1974) and other authors.

$$\min_{\dot{V},c_{SO_2,in},c_{O_2,in},T_{in}} \Phi_{\text{Disc.}} \text{ , with}$$
$$\Phi_{\text{Disc.}} = \sum_{m=2}^{6} \sum_{i=m}^{6} \sum_{j=1}^{5} \left(T_{ns,Mod=m,j} - T_{ns,Mod=i,j}\right)^2 \tag{22}$$

The temperature profiles calculated with the solution of (22) are plotted in Fig. 6. After the experiment is per-

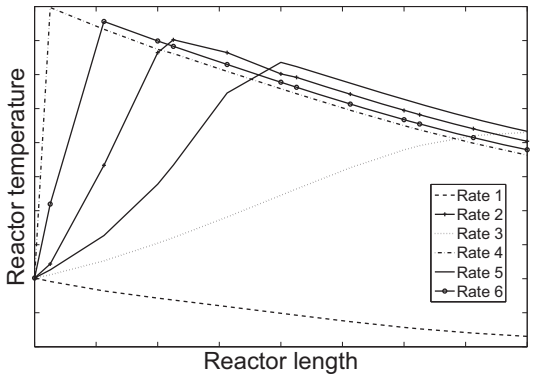

Fig. 6. Model discrimination experiment.

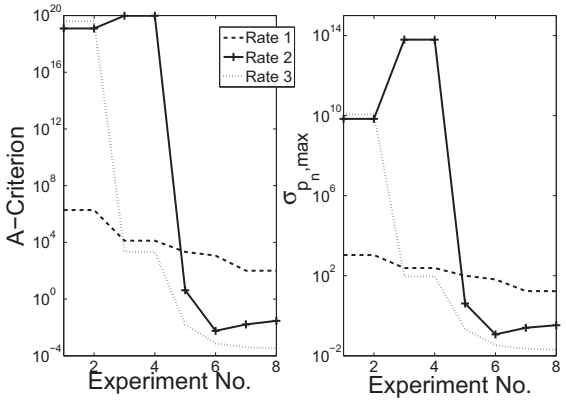

Fig. 7. Development of the parameter accuracy.

formed and the new parameters for each model are found, the profiles are not separated anymore. However, the experiment forces the rate models parameter values to move, and thus, the models flexibility and arbitrariness is reduced considerably.

Only one experiment is designed for a better model discrimination. After the discrimination experiment the rates 1, 2, and 3 are the most promising candidates. The other rates are still considered in the calculations but not plotted anymore in this paper. Further designs for discrimination are not performed because the focus on the parameter accuracy forces also an increasing difference in the models LSQ values. This means that after the convergence of the loop in Fig. 4 a good distinguishability between the rates is reached in addition.

4.3 Nonlinear Optimal Experimental Design Problem

In this work, the A-Criterion is used in order to increase the parameter accuracy, leading to the objective function given in equation (23). A detailed description of the nonlinear optimal experimental design and the different criteria so as a reason for the selection of the A-Criterion can be found in Schöneberger et al. (2008).

$$\min_{\dot{V},c_{SO_2,in},c_{O_2,in},T_{in}} \Phi_{\mathrm{A}}, \text{ with} \quad \Phi_{\mathrm{A}} = \frac{\mathrm{trace}\,(\mathbf{C})}{\dim\,(\mathbf{C})} \tag{23}$$

The covariance matrix of the model parameters $\mathbf{C}$ is approximated with the inverse of the Fisher information matrix $\mathbf{F}$ which can be calculated with equation (24), see Bard (1974). The rate model parameters are summarized in the parameter vector $\mathbf{P}$.

$$\mathbf{C} \geq \mathbf{F}^{-1} = \left[\sum_{j=1}^{NM} \left(\left(\frac{\partial T_{ns,j}}{\partial \mathbf{p}} \right) \frac{1}{\sigma^2_{T_j,T_j}} \left(\frac{\partial T_{ns,j}}{\partial \mathbf{p}} \right)^{\mathbf{T}} \right) \right]^{-1} \tag{24}$$

The parameter's standard deviations $\sigma_{p_n,p_n} = \sqrt{\mathbf{C}(n,n))}$ can be calculated with the diagonal elements of the covariance matrix. The framework is stopped, when a maximal standard deviation of $\sigma_{p_n,p_n,max} \leq 0.02$ is reached. This was accomplished after 8 experiments. The development of the A-Criterion and the maximal parameter standard deviation w.r.t. the experiments is shown in Fig. 7. The development of the LSQ values for the first three rate models

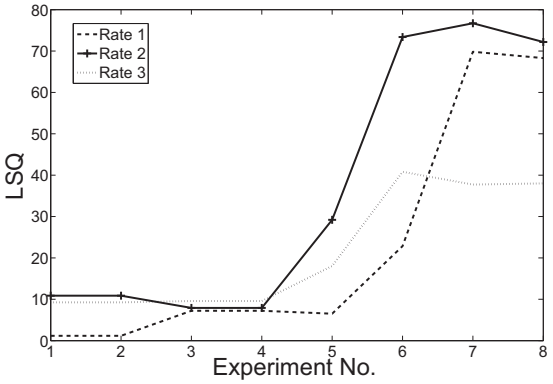

Fig. 8. Development of the lack of fit.

are depicted in Fig. 8. The experiments 1 and 2 and so 3 and 4 are repeated experiments used for the determination of the measured variables standard deviation σ_{T_j,T_j}.

5. RESULTS

In this section, the measured dynamic reactor behavior and the results obtained with the two-phase model are presented.

5.1 Catalyst Properties and Heat Transfer

The specific heat capacity of the catalyst phase $c_{P,k}$ is a model specific property, which has to be determined from experimental data. It should be noted that it is not equal to the heat capacity of the catalysts bulk material since the modeled catalyst phase contains also the particle pores. It can be estimated together with the parameter in the heat transfer correlation from experiments without reaction. This saves reactant gases and reduces the experimental effort because no off-gas treatment is necessary. The transient temperature profiles during the reactor heat up procedure can be used for this issue. They allow the independent estimation of the two parameters because they contain also the initial steady state, when the reactor inlet temperature is reached. These steady state profiles are independent of the catalyst phase heat capacity, but a function of the heat transfer coefficient. In Fig. 9 the numerical solution (surface) is fitted to the measured temperature data (black lines) based on the procedure described in section 4.1.

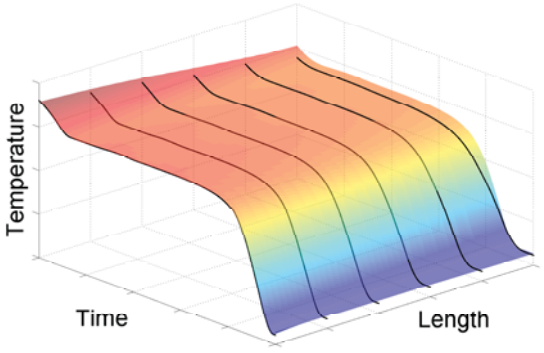

Fig. 9. Time-space surface without reaction.

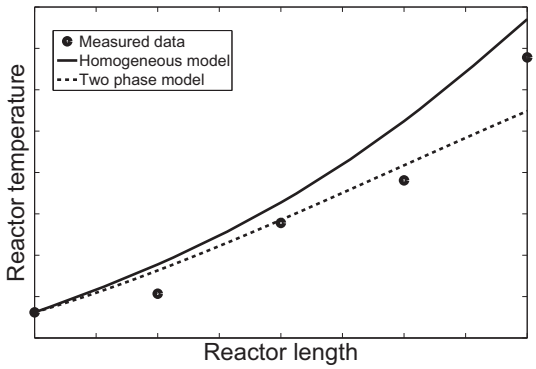

Fig. 10. Steady state comparison of the reactor models.

5.2 Parameter Transfer

Under the assumption of an instantaneous heat and mass transfer and a neglecting of axial dispersion, the model equations of the two-phase model can be rearranged to the form of the homogeneous model in the case of steady state. To show this, the profiles of a solution with the homogeneous model are compared to the steady state solution of the two-phase model in Fig. 10. The differences arise from the stated assumptions, which are not completely fulfilled. However, a steady state examination of a catalyst would not justify the use of the more complex two-phase model.

5.3 Dynamic Reactor Behavior

In Fig. 11, the transient temperature data is plotted. The temperatures after the first and the second bed show a strong overshooting. This behavior can be explained with the two-phase model. The coupled balances for gas and solid phase lead to a PT2 behavior when linearized. This second order element has the potential to produce a swinging solution. The effect is reduced in relation to the distance from the reactor inlet. The last two profiles show inflexion points instead. This can be explained with the increasing reactor wall temperature, which is also disturbing the system as well.

6. CONCLUSIONS

First calculation results show that the two-phase model is able to describe the dynamic reactor behavior. It has been demonstrated that for steady state experiments with a FBR the more complex two-phase model is not required. However, the information content of the transient profiles is much higher than the one from the steady state profiles. The effect on the parameter accuracy still has to be examined, in particular, because of the inclusion of the additional parameters. The knowledge of the dynamic reactor behavior enables the design of optimal transient experiments and their implementation in the proposed identification framework.

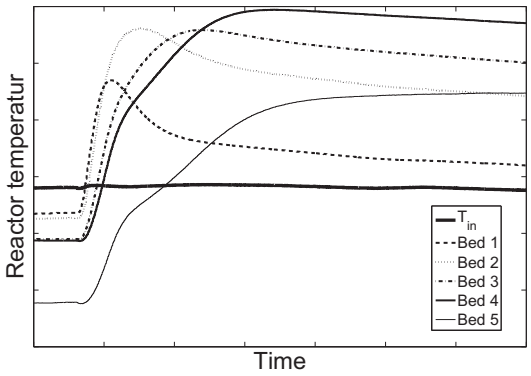

Fig. 11. Transient temperature data with reaction.

ACKNOWLEDGEMENTS

The authors gratefully acknowledge the financial support of the Max-Buchner-Forschungsstiftung, and the provision of the catalyst from the BASF SE.

REFERENCES

Akaike, H. (1974). A new look at the statistical model identification. *IEEE Transactions on Automatic Control*, 19(6), 716–723.

Arellano-Garcia, H., Schöneberger, J.C., and Körkel, S. (2007). Optimale Versuchsplanung in der chemischen Verfahrenstechnik. *Chem. Ing. Tech.*, 79(10), 1625.

Bard, Y. (1974). *Nonlinear Parameter Estimation*. Academic Press, London.

Fogler, H.S. (2006). *Elements of Chemical Reaction Engineering*. Perason International Edition, 4th edition.

Franceschini, G. and Macchietto, S. (2008). Model-based design of experiments for parameter precision: State of the art. *Chem. Eng. Sci.*, 63, 4846.

Mezaki, R. and Kadlec, B. (1972). Remarks on the reduction-oxidation mechanism of sulfur dioxode oxidation on vanadium catalyst. *J. Catal.*, 25, 454.

Schöneberger, J.C., Arellano-Garcia, H., Thielert, H., Körkel, S., and Wozny, G. (2007). An efficient approach to robust simulation of claus processes in coking plants. *Computer Aided Chem. Eng.*, 24, 521.

Schöneberger, J.C., Arellano-Garcia, H., Thielert, H., Körkel, S., and Wozny, G. (2008). Experimental analysis of a fixed bed reactor for catalytic SO2 oxidation. *Ind. Eng. Chem. Res.*, in press.

Schöneberger, J.C., Arellano-Garcia, H., and Wozny, G. (2009). An efficient discretization approach for partial differential equations describing chemical reaction systems. *Computer Aided Chem. Eng.*, in press.